60-GHz LTCC Antenna Arrays

Yong-Xin Guo and Lei Wang

Abstract The wide unlicensed frequency band around 60-GHz for wireless short-range communications are receiving a lot of attention in recent years. As one of the key components in wireless communication systems, the antenna technology affects radio propagation channels, transceiver designs, and choice of digital modulation schemes in establishing a reliable 60-GHz link. In this connection, the 60-GHz antennas for wireless communications, especially antenna-in-package (AiP), have received considerable attention and become a hot research topic. In this chapter, wideband antenna arrays based on the multilayer low temperature co-fired ceramic (LTCC) technology are presented and discussed for 60-GHz wireless short-range communications applications.

Keywords Antenna design · 60 GHz ISM band · 60 GHz radio · IEEE 802.15.3c · LTCC technology · Antenna array

Introduction

The wide unlicensed frequency band around 60 GHz with high data rate characteristic for wireless short-range communications are receiving a lot of attention. For this wireless communication, the data rate of short distance between electronic devices can be realized in multiGbps which is 40–100 times faster than the current WLAN technologies. Communications at the 60-GHz band have lots of advantages such as the possibility of frequency reuse over small distances because of the high attenuation by walls, and the possible miniaturization of the analog components and antennas as the corresponding wavelength in free space is only 5 mm. 60-GHz band wireless short-range communications have a number of applications such as uncompressed high definition video streaming, mobile distributed computing, wireless gaming, fast bulky file transfer, sensing and radar applications, virtually instantaneous access to massive libraries of information, etc. [1].

Y.-X. Guo (✉) · L. Wang
Department of Electrical and Computer Engineering,
National University of Singapore, Singapore, Republic of Singapore
e-mail: eleguoyx@nus.edu.sg

M. R. Yuce (ed.), *Ultra-Wideband and 60 GHz Communications for Biomedical Applications,* DOI 10.1007/978-1-4614-8896-5_11,

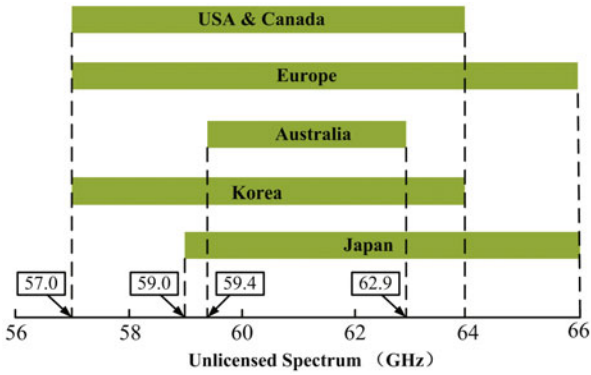

Fig. 1 The spectrum allocation around the 60-GHz band for some countries and regions [3–5]

The IEEE 802.15.3c task group was formed to standardize 60-GHz radios in March 2005, and the IEEE 802.15.3c standard was published in September 2009 to define available and unlicensed frequencies band from 57 to 66 GHz as the 60-GHz band radios applications [2]. The standard divides nearly 9 GHz frequency bandwidth into four 2.16-GHz channels. The Nyquist bandwidth of the standard is 1.632 GHz with a guard bandwidth of 264 MHz on each side to limit spectral leakage. The standard also enforces basic transmission modes: common mode, single-carrier (SC) mode and orthogonal frequency division multiplexing (OFDM) mode. Significant progress has been made in regulations, standards, and solutions. According to the actual situation of countries and regions, different countries and regions have established the 60-GHz regulations for unlicensed utilization, as is shown in Fig. 1. Japan first issued the 60-GHz regulation for unlicensed band from 59 to 66 GHz in the year 2000. The maximum allowable antenna gain of 47 dBi and maximum transmission bandwidth of 2.5 GHz. In 2004, the United States allocated 7 GHz from 57 to 64 GHz for unlicensed use and specified a total maximum transmit power of 500 mW for an emission bandwidth greater than 100 MHz. The 60-GHz regulation in Australia is a narrower 3.5 GHz bandwidth from 59.4 to 62.9 GHz than 7 GHz bandwidth in Japan and USA. The maximum transmit power is limited to 10 mW. A wider 9 GHz bandwidth from 57 to 66 GHz is recommended in Europe. The maximum transmit power of 20 mW, maximum allowable antenna gain of 37 dBi, and minimum transmission bandwidth of 500 MHz are established. Therefore, antennas with wide operating bandwidth to cover more than 9 GHz of the whole 60-GHz bandwidth for different countries and regions applications are desired.

The atmospheric absorption property of sub-terahertz radio spectrum is shown in the Fig. 2. The 60-GHz band is located at the peak point of the oxygen absorption with high attenuation and large propagation loss. The dramatic attenuation at the 60-GHz band is suitable for “whisper radio” short-range wireless communication, where weak signals do not propagate more than a few meters before dropping below the thermal noise level. For 60-GHz wireless communications, the link budget is constrained due to low transmit power (10 mW), large propagation loss (68 dB at 1 m), and high data rate ($\geq$ 1.5 Gb/s). Assuming the 10-mW value for the average

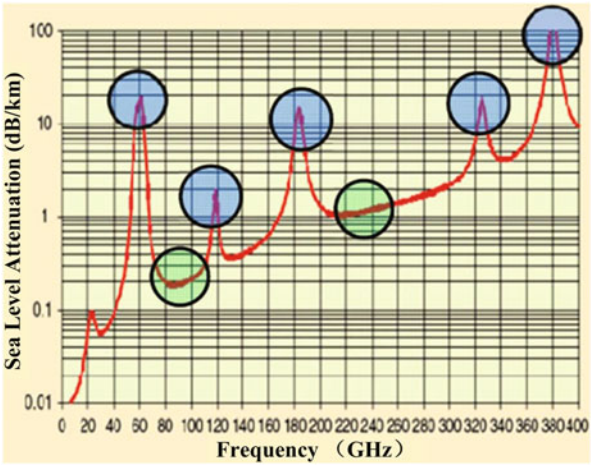

Fig. 2 The properties of atmospheric absorption of electromagnetic waves [4]

transmitter power for portable devices, a gain of ∼ 15 dBi is usually required for 60-GHz indoor WLAN applications. Hence, the use of antenna arrays with high-gain is anticipated.

Low-temperature co-fired ceramic (LTCC) multilayer technology enables integration of passive components including antennas in a single package. Compared with the multilayer print circuit board (PCB) technology, the LTCC technology is capable of realizing blind, buried and through vias and air cavities in the substrate easily [6]. The LTCC technology is also allowed to mount active devices or integrated circuit on/in them to achieve a new option to integrate an antenna array in a chip package. Several LTCC materials can be selected. Ferro A6 is one kind of LTCC material suitable for 60-GHz antenna array design, due to its excellent high frequency characteristic. Based on the Ferro A6 material, LTCC technologies can realize functional packages and antennas for applications in the 60-GHz band. The LTCC process has been regarded the promising technology of achieving light weight, compactness, easy integration, and excellent high frequency performance for 60-GHz wireless communication applications.

Considering the wide 15 % bandwidth (for 9 GHz world wide band coverage) and more than 15 dBi gain requirements, the antenna arrays based on LTCC technology have many challenges for 60-GHz wireless short-range communications. Due to the high permittivity of the LTCC substrate, the bandwidth of antenna arrays is limited. Hence, the choice of the array element becomes more significant for 60-GHz antenna array design. A variety of array elements, such as patch, dipole, slot, and others have been used as the element in the 60-GHz LTCC antenna array designs. Also some methods about broadening bandwidth of the LTCC antennas have been reported, such as using aperture coupled patch, U-slot patch, L-probe patch, stacked patch, and off-center dipole, etc. [7–13]. For the antenna arrays, the feeding network is crucial to develop the antenna arrays. A parallel, series, or combined feed is used to produce the necessary amplitude and phase distribution for an array element.

Compared with a series feed, a parallel feed can offer a wider bandwidth. Several types of transmission line can be used as the feeding network, such as microstrip line, stripline (SL), coplanar waveguide (CPW), substrate-integrated waveguide (SIW), or hybrid structures. However, the gain of the antenna array is limited by the loss caused by its feeding network, such as a microstrip line, especially at the 60-GHz band applications. Stripline and SIW with lower transmission loss and better isolation than microstrip line have been widely employed at the 60-GHz LTCC antenna array designs.

Furthermore, due to the higher permittivity of LTCC substrate, the surface wave could introduce significant loss in LTCC antenna array design at millimeter-wave 60-GHz bands. Enhancing the gain performance of the 60-GHz antenna array based on LTCC technology becomes much more challenging. The strong surface wave propagation is the primary reason of producing the mutual coupling between the elements. Some methods of suppressing the surface-wave loss to reduce the mutual coupling and enhance the gain of the LTCC antenna have been reported, such as embedding an air cavity inside the substrate, removing the partially substrate around the radiating elements, loading the uniplanar-compact electromagnetic band-gap (UC-EBG), loading the artificial soft-surface structure, using open-ended SIW cavity structure, and using metal-top via fence structure, etc. [14–18].

In this chapter, the antenna arrays based on LTCC technology for 60-GHz short-range wireless communication applications are presented. The antenna elements and compact feeding networks for achieving different polarization performances of the antenna arrays are studied. For measurement, the transition of the grounded coplanar waveguide (GCPW) to the SL is designed based on LTCC multilayer structure. Also, for suppressing the surface wave propagation in the array, the soft-surface structure, and open-ended SIW cavities are used to improve the radiation performance of antenna arrays with different polarization characteristic. The antenna arrays with compact structure and good performance, including a wideband linearly polarized L-probe feed patch antenna array with soft-surface structure, and a dual-polarized L-probe feed patch antenna array with open-ended SIW cavities structure are presented and studied.

60-GHz LTCC Linearly Polarized Antenna array

A 4×4 L-probe patch linearly polarized antenna array with a soft-surface structure using multilayer LTCC technology is presented for 60-GHz band applications. The technique of employing an L-shaped probe to feed a thick patch antenna for achieving a wideband antenna of bandwidth $> 30\,\%$ has been widely reported [19–21]. However, all these antennas were designed on traditional substrate materials, and the operating frequency bands were below 10 GHz. The L-probe feed patch antenna as an element is designed and fabricated using LTCC technology at 60-GHz band. On the other hand, the artificially soft-surface structure was employed to improve antenna performance as it can force the field intensity for any polarization to be

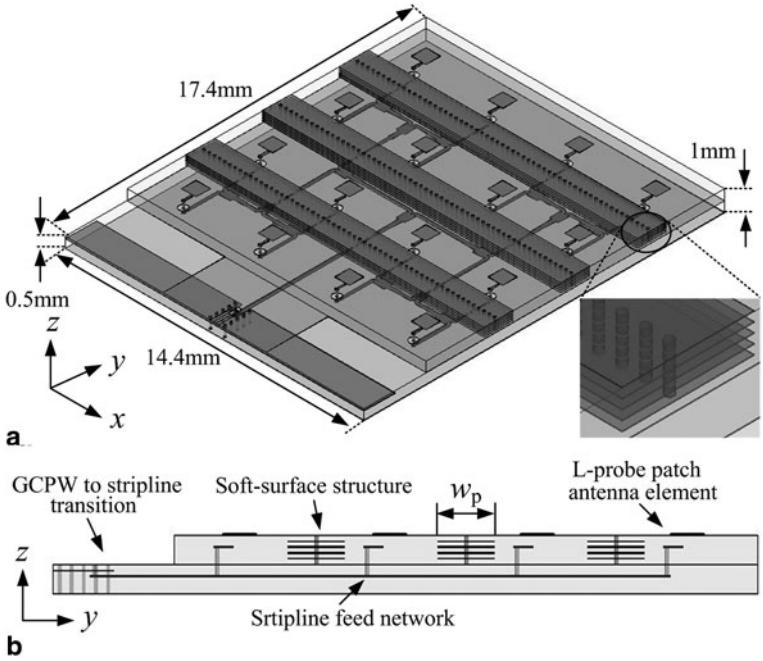

Fig. 3 Geometry of the proposed low temperature co-fired ceramic (LTCC) based L-probe patch array with novel soft-surface structures. **a** 3D view, **b** *side* view (from [10], reprinted with permission from IEEE)

zero on the surface for wave propagating along the surface [22–24]. A novel soft-surface structure is introduced in the LTCC L-probe antenna array to suppress the substrate surface wave and thus enhance the antenna array radiation performance without increasing the overall size and requiring additional process. The proposed antenna array is fed by a SL feed network to separate from the radiation elements. The effects of the soft-surface structure on the performance of antenna array are numerically and experimentally investigated by comparing with the conventional L-probe patch linearly polarized array without the soft-surface structure.

Overview of the Antenna Array

A planar array of 4 × 4 L-probe patch antenna elements with a novel soft-surface structure was designed. The proposed antenna array is composed of 16 L-probe fed patch antenna elements; T-junction feeding network, and GCPW to SL transition for probe station testing as shown in Fig. 3. Three novel soft-surface structures constituted of metal strips on each layer and via fences were inserted in the middle of the antenna array along the x-axis. The value of w_p is the metal strip width of the proposed soft-surface structure. The via fences are composed of a row of vias.

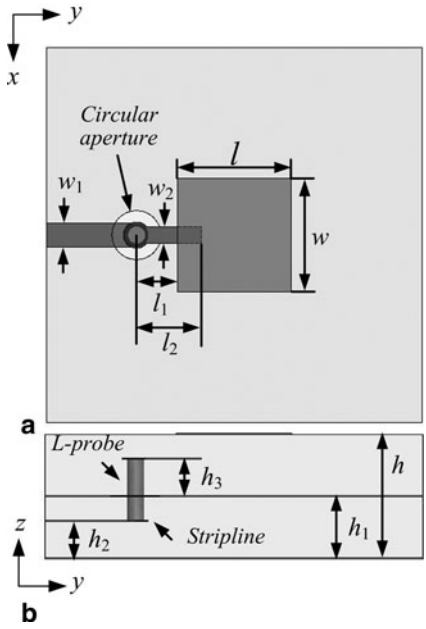

Fig. 4 Geometry of the LTCC L-probe patch element. **a** *Top* view, **b** *Side* view (from [10], reprinted with permission from IEEE)

Following the fabrication process requirement, the diameter of each via is 0.1 mm, and the distance between the centers of two adjacent vias is 0.25 mm. In this work, the element spacing of $d = 3.7$ mm ($0.75\lambda_0$) was chosen. The total size of the proposed antenna array excluding the measurement transition is $14.4 \times 14.4 \times 1\,\text{mm}^3$.

Single L-probe Patch Radiating Element

The single L-probe patch antenna element is shown in Fig. 4. The multilayer LTCC substrate used is Ferro A6-M with dielectric permittivity $\varepsilon_r = 5.9$ and loss tangent $\tan\delta = 0.001$. The conductor thickness is $t = 0.01$ mm. The L-probe is constituted by a vertical via and a horizontal microstrip line. The proposed antenna element is fed by a SL to suppress the radiation from the feeding line. The detailed dimensions are shown in Table 1. The total thickness h is 1 mm (10 LTCC layers) including five LTCC layers (0.5 mm) as the SL feeding part and five LTCC layers (0.5 mm) as the antenna part. The width w_1 of the feed SL was chosen to be 0.15 mm, which corresponds to the characteristic impedance of 50 Ω. The via diameter is 0.1 mm.

Figure 5 shows the simulated impedance bandwidth and gain of the proposed antenna element by HFSS. The simulated impedance bandwidth is about 50.4 % with respect to the center frequency of 61.5 GHz from 46 to 77 GHz for $|S_{11}| \leq -10$ dB. The simulated gain is 5.7 dBi at 60 GHz.

Table 1 Detailed L-probe patch antenna element dimensions

Parameters	Dimensions (mm)	Parameters	Dimensions (mm)	Parameters	Dimensions (mm)
w	0.7	w_1	0.15	l	0.7
w_2	0.1	l_1	0.25	l_2	0.4
h	1	h_1	0.5	h_2	0.3
h_3	0.3				

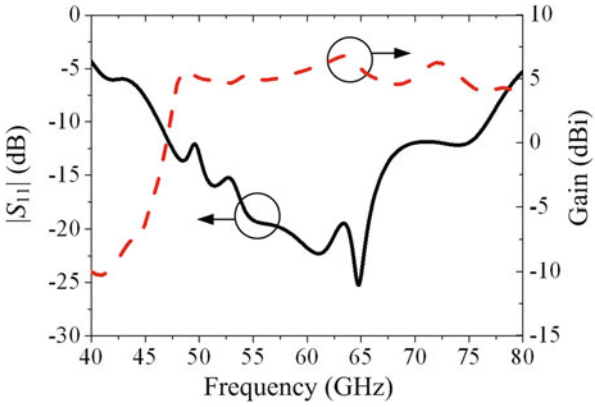

Fig. 5 Simulated $|S_{11}|$ and gain of the single element (from [10], reprinted with permission from IEEE)

Feeding Network and GCPW-SL Transition

A quarter-wave T-junction power divider was used as a feed network to split the power equally. From 48 to 70 GHz, the simulated insertion loss of the T-junction is less than 0.3 dB and simulated $|S_{11}|$ is better than -20 dB.

A (GCPW to SL transition was designed on LTCC so that the antenna array can be measured with the probe station measurement as illustrated in Fig. 6. A partial middle ground which is lower than the upper ground by 0.1 mm to facilitate the probe pitch touching. The simulated $|S_{11}|$ is below -18 dB and $|S_{21}|$ is less than -0.15 dB from 40 to 70 GHz.

Investigation of Antenna Array with Soft-surface

The Effect of the Soft-surface Structure Metal Strips Width

The antenna array with different metal strip width of the soft-surface structure: $w_p =$ 0.4, 0.8, 1.4, and 2.0 mm are simulated to study its influence on the performance of the antenna array. The comparisons of the simulated $|S_{11}|$ and gain with different w_p are shown in the Fig. 7. It is seen that both the impedance and radiation performance are related to the width of the soft-surface structure obviously. When w_p is smaller than 0.4 mm, the impedance matching of the antenna array is poor and the gain is

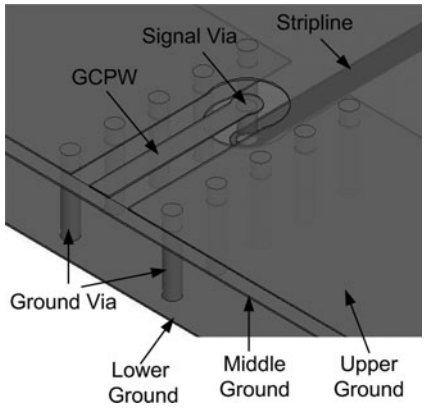

Fig. 6 Geometry of the grounded co-planar waveguide (GCPW) to SL transition (from [10], reprinted with permission from IEEE)

not improved. The antenna is well matched and the antenna gain can be improved significantly when $w_p = 0.8$ and 1.4 mm. But, when the width of the soft-surface structure is big enough to affect the antenna radiation, the impedance becomes worse again. After optimization, considering the simulated $|S_{11}|$ and gain, the value of w_p is chosen to be 1.4 mm.

The Effect of the Soft-Surface Structure Location

To understand the effectiveness of the soft-surface structure location, we simulated the $|S_{11}|$ and gain of the antenna array for three different types of the soft-surface structure locations: along x-axial as the Fig. 8a, along y-axial as the Fig. 8b, and along both x-axial and y-axial as the Fig. 8c, respectively.

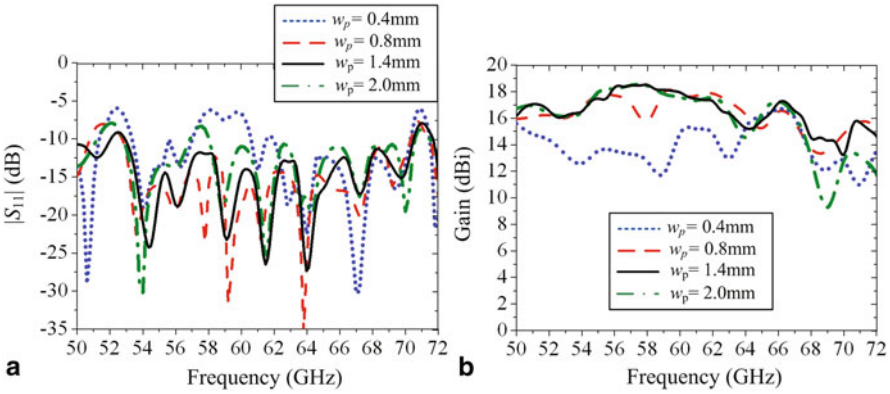

Fig. 7 Comparison of simulated $|S_{11}|$ and gain with different w_p. **a** Simulated $|S_{11}|$, **b** Simulated gain (from [10], reprinted with permission from IEEE)

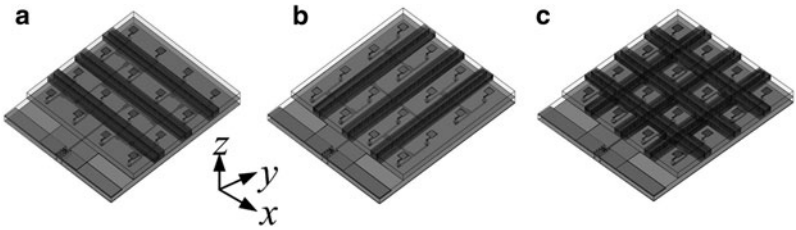

Fig. 8 Geometry of three antenna arrays with different locations of the soft-surface structure, **a** Along *x*-axial, **b** Along *y*-axial, **c** Along both *x*-axial and *y*-axial(from [10], reprinted with permission from IEEE)

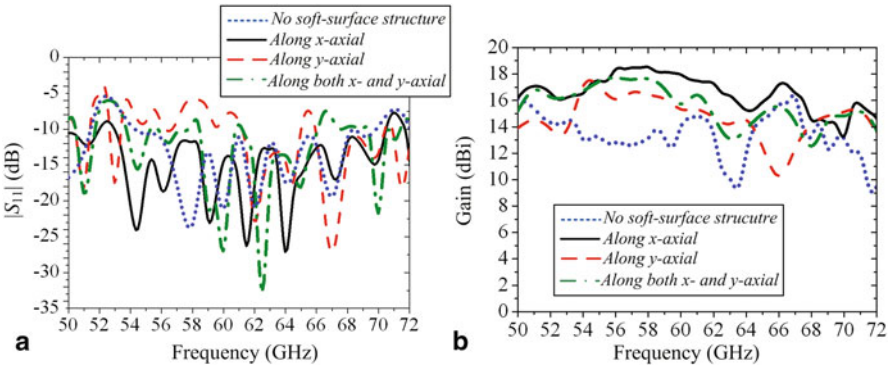

Fig. 9 Comparison of simulated $|S_{11}|$ and gain with different locations. **a** Simulated $|S_{11}|$, **b** Simulated gain (from [10], reprinted with permission from IEEE)

The simulated $|S_{11}|$ and gain of the soft-surface structure at different locations are compared in Fig. 9. The simulated results of the conventional L-probe patch antenna array without any soft-surface structure are also shown as a reference. If the soft-surface structure is changed to be along the *y*-axis as in Fig. 8b, the impedance is mismatched seriously, and the gain is not improved as significantly as the case with soft-surface structure along the *x*-axis as in Fig. 8a. The reason is that the coupling along *y*-axis between antenna elements are stronger than that along *x*-axis. For the case with soft-surface structures along both *x*-axis and *y*-axis, as in Fig. 8c, the impedance matching becomes worse to result in lower gain than that for the case with soft-surface structures only along *x*-axis. Both good impedance and radiation performance of the antenna array can be achieved by placing the soft-surface structure just along the *x*-axis.

Antenna Arrays With or Without the Soft-surface Structure

Figure 1 shows the 3D view and side view geometry figures of the three different types of antenna arrays with or without the novel soft-surface structure, respectively. Design I shown in Fig. 10a is the L-probe patch antenna array without any soft-surface structure. Design II shown in Fig. 10b is the L-probe patch antenna array with

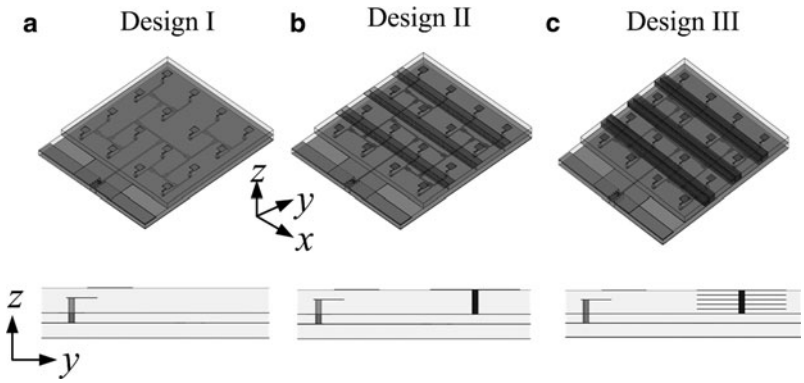

Fig. 10 Geometry of three different L-probe patch antenna arrays with or without the soft-surface structure. **a** Array without the soft-surface structure, **b** Array with the soft-surface structure of one layer, **c** Array with the soft-surface structure of each layer (from [10], reprinted with permission from IEEE)

the soft-surface structure of the metal strip only on the top layer. Design III shown in Fig. 10c is the L-probe patch antenna array with the proposed soft-surface structure of the metal strips on each layer to guarantee the good connection of the vias at different layers. To simplify the simulation, all the metal strips have the identical width of $w_p = 1.4$ mm on each layer. To demonstrate the effectiveness of the proposed novel soft-surface structure inserted in the antenna array for the impedance and radiation performance improvement, simulated results for the above three cases were presented for comparison.

The simulated results show that the impedance and radiation performance are almost the same for Designs II and III, which indicates that only the top metal strip has the primary influence on the performance. The metal strips at the other layers which are used to guarantee the good connection of the vias have little effect as long as the width of those strips are not bigger than that of the top metal strip (w_p).

Figure 11a compares the simulated $|S_{11}|$ of the antenna arrays with or without the soft-surface structure. The bandwidths of the arrays without and with the soft-surface structure for $|S_{11}| < 10$ dB are 27 % (Design I) and 29 % (Design III), respectively. The impedance bandwidth of the antenna array seems not sensitive to the soft-surface structure, and the bandwidth is improved for the array with the soft-surface structure slightly. From Fig. 11b, the simulated peak gain around 60 GHz of the antenna array with the soft-surface structure (Design III) is near 18 dBi, which is about 4 dBi higher than that of the array without the soft-surface structure (Design I). Also, compared with the antenna array without the soft-surface structure (Design I), a more stable peak gain is achieved by adding the soft-surface structure in the operation band.

The radiation patterns of different antenna arrays with or without the soft-surface structure in two principal planes at 60 GHz are compared in Fig. 12. It is seen that the antenna array without the soft-surface structure (Design I) has a worse sidelobe radiation due to the contribution from the surface wave diffraction. As we know, the L-probe patch antenna has a poor cross polarization at the H-plane. By introducing the

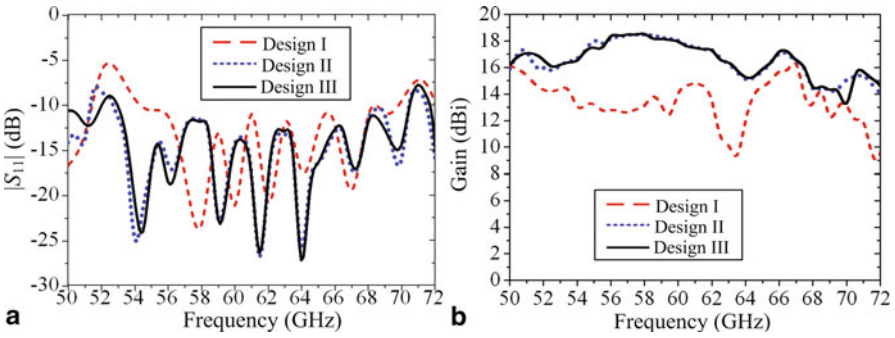

Fig. 11 Comparison of simulated $|S_{11}|$ and gain among three cases, **a** Simulated $|S_{11}|$, **b** Simulated gain (from [10], reprinted with permission from IEEE)

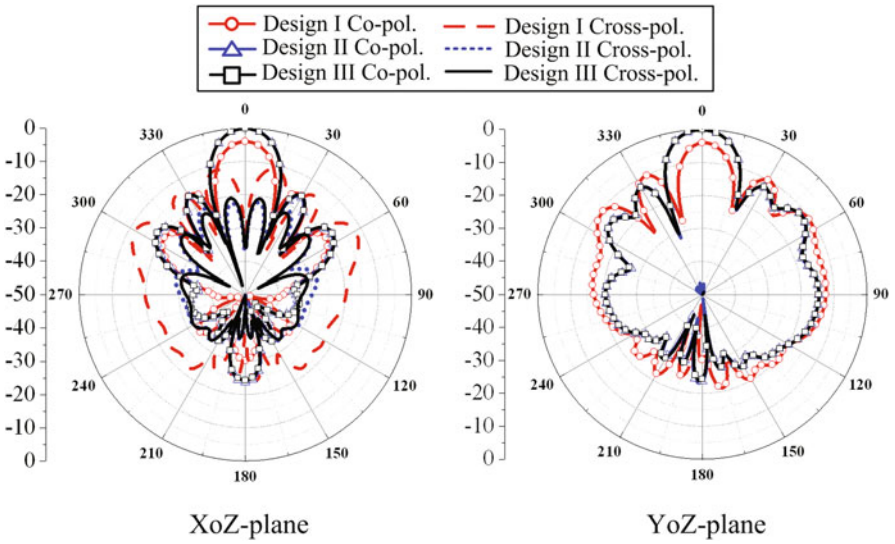

Fig. 12 Comparison of simulated radiation patterns between three different arrays at 60 GHz (from [10], reprinted with permission from IEEE)

soft-surface structure, the radiation performance is significantly improved, including enhanced radiation field in the maximum radiation direction, lower cross polarization of the H-plane, and reduced sidelobe radiation.

Mechanism for Performance Enhancement of Antenna Array by the Soft-surface Structure

In order to investigate the mechanism for the novel soft-surface structures placed in the antenna array, the electric field distributions on the top surface of the substrate for the middle two-row eight elements of the antenna array simulated by HFSS are shown in Fig. 13.

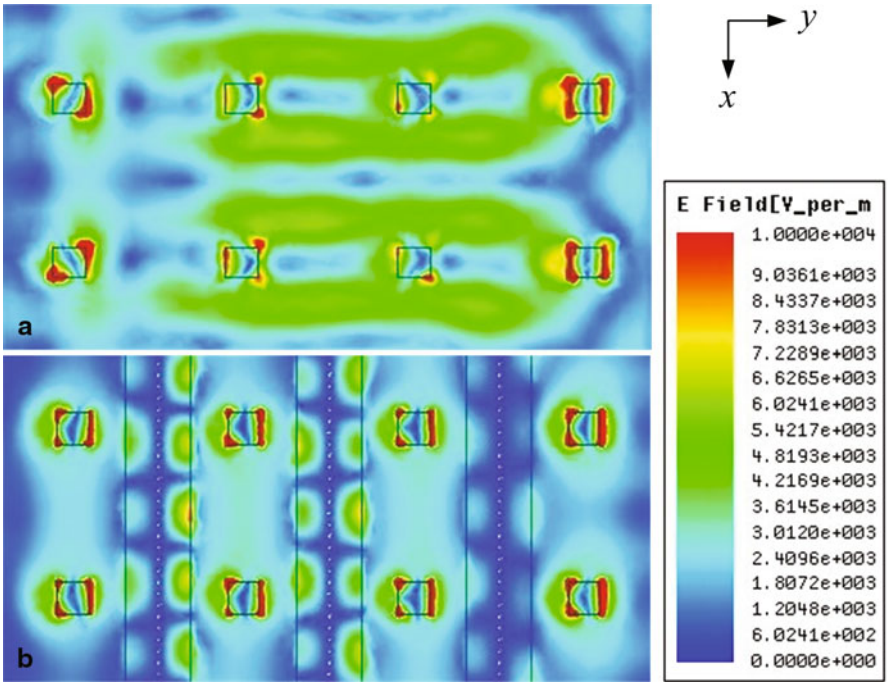

Fig. 13 Simulated electric field distributions on the *top* surface of the substrate for the *middle* two-row eight elements of the antenna array with and without the soft-surface structure. **a** Without the soft-surface structure, **b** With the soft-surface structure (from [10], reprinted with permission from IEEE)

When the antenna is fabricated on a large-size substrate with higher dielectric constant, the radiation performance will be much affected by the diffraction of surface waves. As Fig. 13a shows, there is a strong electric field from the surface waves in the area between the antenna elements, in particular along the *y*-axis. As the intrinsic electric field of the L-probe patch antenna element is heavily affected by the strong surface waves, the radiation performance of antenna array is deteriorated. The proposed soft-surface structure with the shorted metal strip and via fence blocks the surface wave propagates. As a result, the surface waves can be substantially suppressed; hence, the radiation performance of antenna array is improved. To confirm this finding by checking the field distribution in the substrate shown in Fig. 13b, we can see that the surface waves is suppressed in the substrate and the field distribution of the L-probe radiation patch is improved obviously.

The other factor contributing to the radiation performance improvement is the fringing field along the metal strips of the proposed soft-surface structure. As Fig. 13b shows, the fringing field along the metal strips forms a radiation array. The formed array acts as a broadside array. Although the magnitude of the fringing field along the soft-surface structure is much lower than radiating edge of the L-probe patch antenna, the size of the soft-surface structure is much larger than the patch. As a result, the contribution from the soft-surface structure to improve the performance of antenna array is significant.

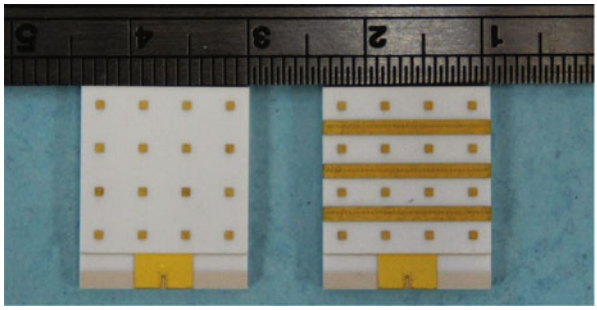

Fig. 14 Photographs of the proposed antenna arrays. *Left* without the soft-surface structure. *Right* with the soft-surface structure (from [10], reprinted with permission from IEEE)

Experimental Results

Figure 14 exhibits the photographs of the fabricated L-probe patch antenna arrays without and with the novel soft surface using LTCC process, respectively.

Figures 15 and 16 compare the measured and simulated $|S_{11}|$ and gain of the antenna array without and with the soft-surface structures, respectively. The measured frequency band ranged from 50 to 67 GHz is limited by the test cable and adapter. The measured and simulated results are in good agreement. The simulated impedance bandwidth for $|S_{11}| < -10$ dB are as follows: 26.7 % with respect to the center frequency of 61.7 GHz (from 53.5 to 70 GHz) for the antenna array without the soft-surface structure, and 29 % with respect to the center frequency of 62 GHz (from 53 to 71 GHz) for the array with the soft-surface structure, respectively. The measured $|S_{11}|$ of the frequency ranges from 51 to 67 GHz for the array without the soft-surface structure and from 51.5 to 67 GHz for the array with the soft-surface structure are all below −10 dB.

The simulated and measured gain values are 14 and 13.4 dBi for the antenna array without the soft-surface structure, and 18 and 17.5 dBi for the array with the soft-surface structure at 60 GHz, respectively. The measured 3-dB gain bandwidth

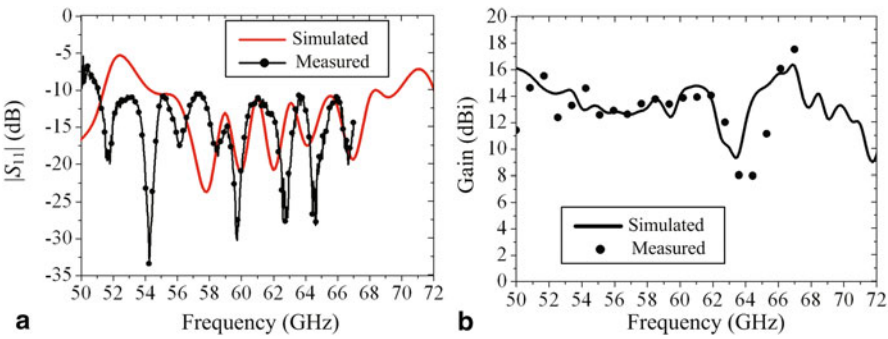

Fig. 15 Measured and simulated $|S_{11}|$ and gain of the antenna array without the soft-surface structure. **a** $|S_{11}|$, **b** Gain (from [10], reprinted with permission from IEEE)

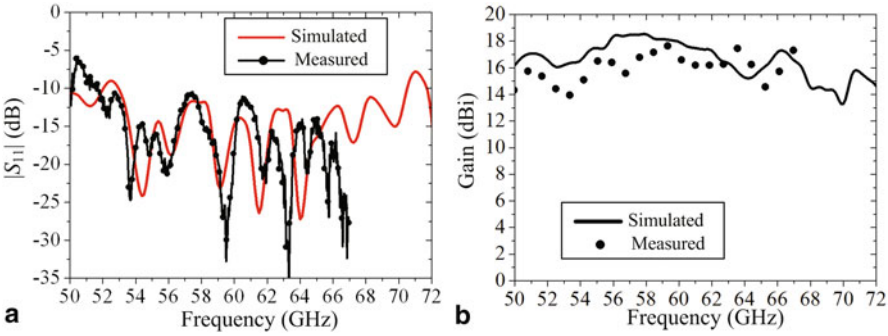

Fig. 16 Measured and simulated $|S_{11}|$ and gain of the antenna array with the soft-surface structure. **a** $|S_{11}|$, **b** Gain and efficiency (from [10], reprinted with permission from IEEE)

of the array with the soft-surface structure is from 54.5 to 65.5 GHz. The gain of the array with the soft-surface structure is about 4 dB higher than that of the array without the soft-surface structure at 60 GHz. This is because stronger surface wave introduced by the thicker substrate and high dielectric constant makes the radiation in the broadside worse for the case without the soft-surface structure. By adding the soft-surface structure in this design, the surface wave is suppressed significantly.

The measured and simulated co-pol and cross-pol radiation patterns of the L-probe patch antenna array with the soft-surface structure in two principal planes (XoZ-plane and YoZ-plane) at the frequencies of 55, 60, and 65 GHz are shown in Fig. 17, respectively. The measured HPBW is about 20° in two principal planes at 60 GHz. The measured cross-polarization level is almost 20 dB below the corresponding co-polarization at 60 GHz. Slight discrepancies between the simulated and measured results are mainly caused by the fabrication tolerance and possible effect of the test setup.

A 4 × 4 LTCC L-probe patch linearly polarized antenna array with a novel soft-surface structure is presented and tested for 60-GHz wireless communication applications. The introduced soft-surface structure has suppressed the surface wave significantly. The proposed antenna array features wide impedance bandwidth, high gain and stable gain bandwidth.

60-GHz LTCC Dual-Polarized Antenna array

A 60-GHz dual-polarized 4 × 4 L-probe patch antenna array based on LTCC technology is presented. Few efforts have been made for a polarization diversity antenna which is an important issue in a mobile or portable wireless communication system. A dual-polarized antenna can provide polarization diversity to reduce the multipath fading of the received signals or furnish frequency reuse to double the capacities [25–29]. A "differential feed" approach is adopted to realize the dual polarization in this work. The L-probe feed patch antenna is designed and fabricated using LTCC technology at the 60-GHz band to achieve wideband impedance bandwidth. A compact multilayer SL feeding network structure is employed to realize the dual

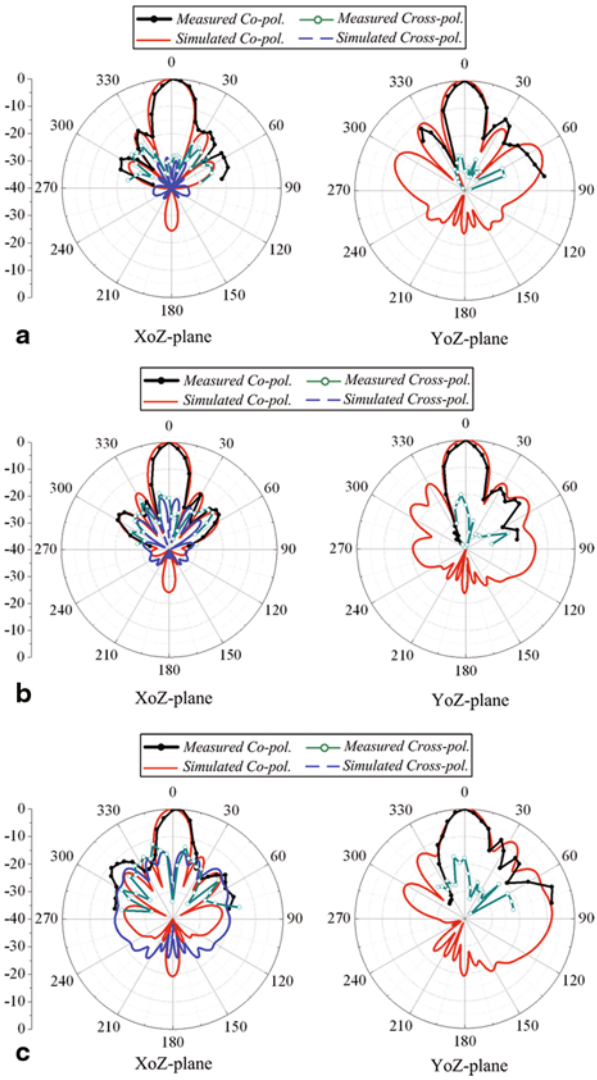

Fig. 17 Measured and simulated radiation patterns of the antenna array with the soft-surface structure. **a** 55 GHz, **b** 60 GHz, **c** 65 GHz

polarization characteristic of the array. The open-ended substrate integrated cavities (SICs) structure is embedded in the antenna array without increasing the overall size and requiring additional process to suppress the substrate surface wave and enhance the gain. A 4 × 4 dual-polarized L-probe patch antenna array in LTCC technology with the open-ended SICs is built and demonstrated for 60-GHz wireless communication applications.

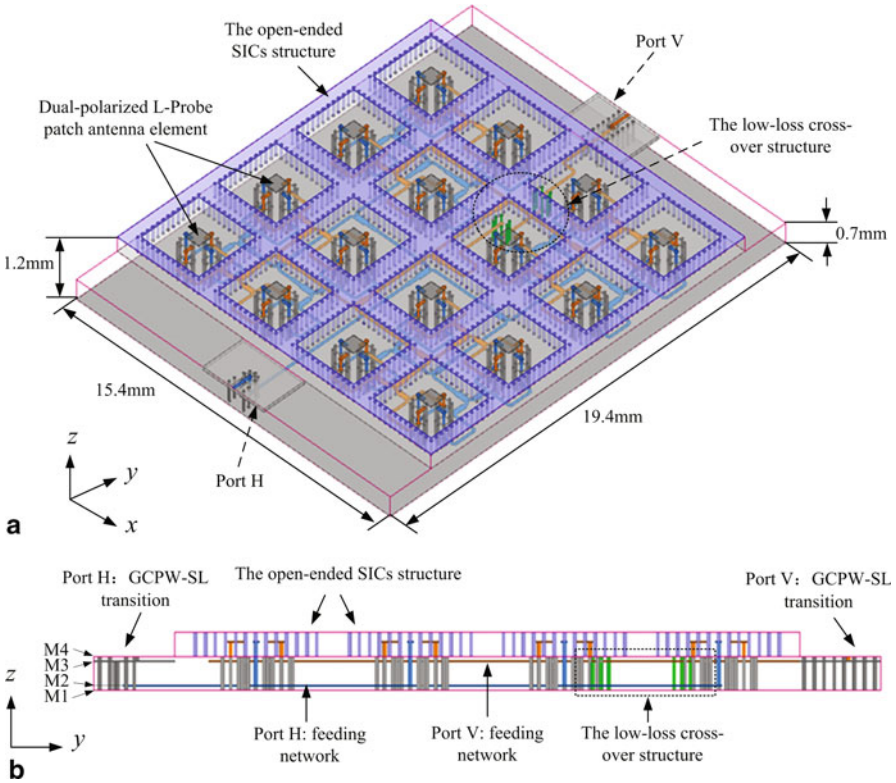

Fig. 18 Geometry of the proposed dual-polarized L-probe patch array with the open-ended SICs. **a** 3D view, **b** *Side* view

Overview of the Antenna Array

A 4 × 4 dual-polarized L-probe patch antenna array using "differential feed" approach with the open-ended SICs is designed and implemented for 60-GHz applications. The configuration of the proposed antenna array is shown in Fig. 18. The proposed antenna array is composed of 16 "differential feed" L-probe antenna elements, compact dual polarization SL feeding network, the open-ended SICs, and two GCPW to SL transitions for probe station testing. The element spacing of two adjacent patches is 3.8 mm (0.76 λ_0). The total size of the proposed antenna array excluding the measurement transitions is 15.4 × 15.4 × 1.2 mm^3.

Antenna Element Design and Investigation

Investigation of "Differential Feed" Approach for Isolation Enhancement

Figure 19 shows the geometry of the two antenna elements with different feeding approaches. Element A, as shown in Fig. 19a, uses the conventional "single feed"

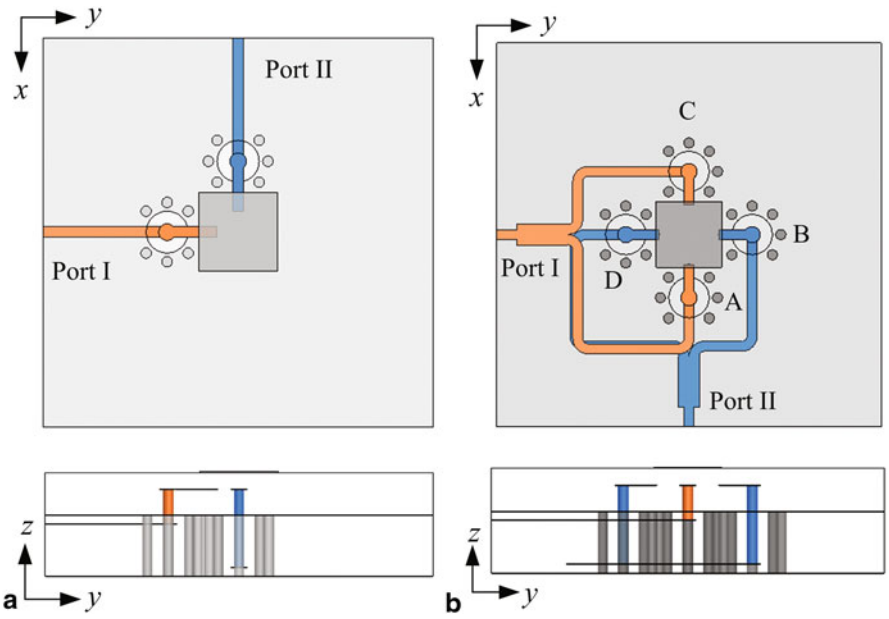

Fig. 19 Geometry of two antenna elements with different feeding technology. **a** Element A: "single feed" approach, **b** Element B: "differential feed" approach

approach. Two orthogonal L-probes as two input ports excite the patch to achieve dual polarization characteristic. In Fig. 19b, Element B illustrates the "differential feed" approach. Four mutual orthogonal L-probes are employed to excite the patch. Probes A and C along x-axis connected to the balun with 180° phase difference of two outputs as Port I are used to excite horizontal polarization, and Probes B and D along y-axis connected to the balun with 180° phase difference of two outputs as Port II are used to excite vertical polarization. Here, we define that horizontal polarization is the polarized direction along the x-axis and vertical polarization is the polarized direction along the y-axis. The signal via of the L-probe is surround by a circle of shielding vias which are composed of six vias connected the top and bottom ground of the SL structure. The shielding vias positioned around the apertures can achieve an optimum coaxial effect to ensure a low transmission loss of the signal via [30, 31].

Figure 20 shows the simulated S parameters of the proposed two antenna elements. For the element A, as Fig. 20a shows, the simulated impedance bandwidth in the frequency range is from 51.5 to 70 GHz for Port I ($|S_{11}| < -10$ dB) and from 53.5 GHz to simulation upper limit frequency 75 GHz for Port II ($|S_{22}| < -10$ dB). For Element B, as Fig. 20b shows, the simulated 10-dB bandwidth is about 25.4 % with respect to the center frequency of 60.5 GHz from 52.5 to 68.5 GHz for Port I ($|S_{11}|$) and about 30.2 % with respect to the center frequency of 63 GHz from 53.5 to 72.5 GHz for Port II ($|S_{22}|$), respectively.

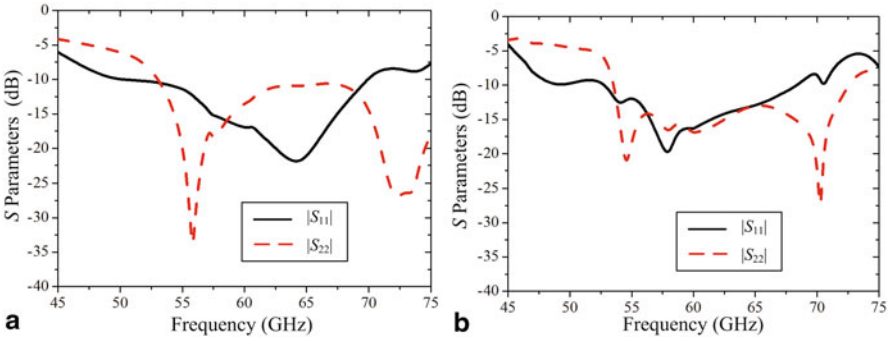

Fig. 20 Simulated *S*parameters with different feed technologies. **a** Simulated $|S_{11}|$ and $|S_{22}|$ for Element A, **b** Simulated $|S_{11}|$ and $|S_{22}|$ for Element B

Fig. 21 Simulated isolation against frequency for Element A and Element B

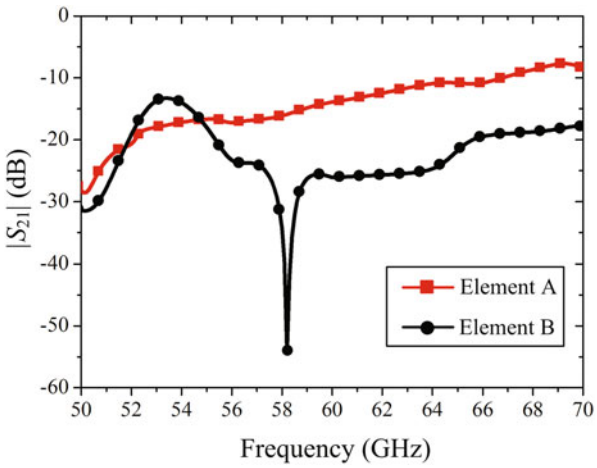

Figure 21 shows the simulated $|S_{21}|$ for Element A and Element B. It is clearly seen that the $|S_{21}|$ of Element A is about −15 dB around 60 GHz, and the corresponding $|S_{21}|$ of Element B is less than −25 dB form 55 to 65 GHz. The 10 dB improvement of the isolation is contributed by the "differential feed" approach obviously. It is because that the poor isolation in Element A is mainly due to the strong coupling between two vertical via portions of the L-probes. However, for Element B which employs the "differential feed" approach, the probes A and C are excited with 180° phase difference, while the probes B and D are also excited with 180° phase difference. The coupling between the probes A and B can be cancelled by the coupling between the probes A and D. Similarly, the coupling between the probes C and B can be cancelled by the coupling between the probes C and D with equal magnitude but 180° out of phase. For this reason, applying the "differential feed" approach can improve the isolation significantly.

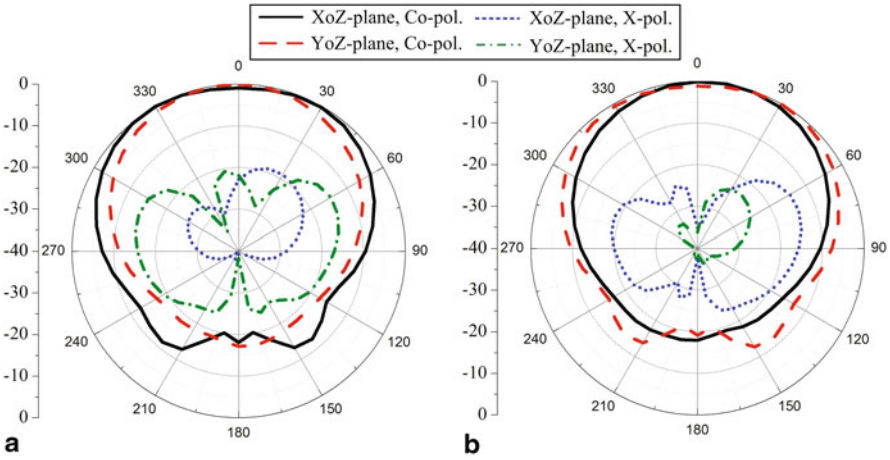

Fig. 22 Simulated radiation pattern for Element B at 60 GHz. **a** Port I: *horizontal* polarization, **b** Port II: *vertical* polarization

The simulated radiation pattern at 60 GHz for Element B is shown in Fig. 22. For Port I, the 3-dB beamwidths are 110 and 90° in XoZ- and YoZ-plane, respectively. The corresponding values for Port II are 80 and 120°. The back-lobe levels for both the horizontal and vertical polarizations are about −18 dB. The simulated gain of Element B are 5.3 dBi for Port I and 5.15 dBi for Port II at 60 GHz, respectively.

The Effect of the Open-Ended SICs on the Antenna Element

The proposed dual-polarized L-probe patch antenna element with the open-ended SIC is shown in Fig. 23. The distance between the power divider feeding network as the Port I and the bottom metal ground of SL structure is h_2. Whereas the distance between the power divider feeding network as the Port II and the bottom metal ground of SL structure is h_3. The multilayer SL as the feeding network structure can be of compact size and suppress the radiation from the feeding line. The open-ended SIC structure is loaded around the L-probe feed dual-polarized antenna element. It is composed of topped metal strip and metal vias fence constituted by a circle of vias. The distance *cd* between the centers of two adjacent vias is 0.25 mm. The width of the feed SL was chosen to be 0.1 mm, which corresponds to the characteristic impedance of 50 Ω. The detailed dimensions of the proposed dual-polarized antenna element are shown in Table 2.

The simulated *S* parameters of the antenna element with the open-ended SIC are shown in Fig. 24 compared with the performances of the antenna element without the open-ended SIC (Element B). For the antenna element with the open-ended SIC, as the Fig. 24a shown, the simulated impedance bandwidth is about 27.5 % with respect to the center frequency of 63.25 GHz from 54.5 to 72 GHz for Port I ($|S_{11}| < -10$ dB) and about 32.2 % with respect to the center frequency of 63.75 GHz from 53.5

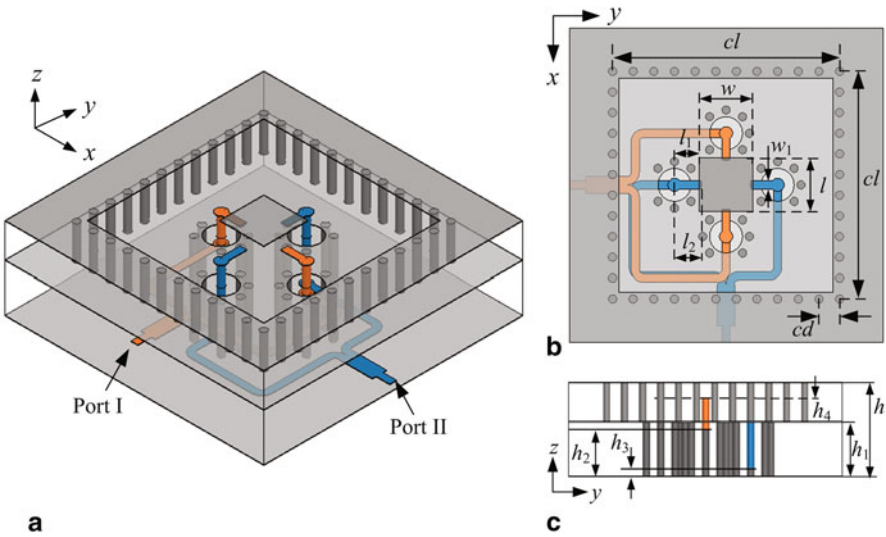

Fig. 23 Geometry of the proposed LTCC dual-polarized L-probe patch antenna element. **a** 3D view, **b** *Top* view, **c** *Side* view

Table 2 Detailed dual-polarized antenna element dimensions

Parameters	Dimensions (mm)	Parameters	Dimensions (mm)	Parameters	Dimensions (mm)
w	0.7	w_1	0.1	l	0.7
l_1	0.25	l_2	0.3	cl	2.7
cd	0.25	h	1.2	h_1	0.7
h_2	0.6	h_3	0.1	h_4	0.3

to 74 GHz for Port II ($|S_{22}| < -10$ dB), respectively. Compared with the element without the open-ended SIC, the impedance bandwidth of the antenna element with the open-ended SIC is improved slightly. The simulated $|S_{21}|$ of the proposed antenna element with the open-ended SICs is less than −25 dB form 56 to 65 GHz.

Figure 25 shows the simulated radiation pattern at 60 GHz for the proposed antenna element with the open-ended SIC. For Port I, the 3-dB beamwidths are 95 and 75° in XoZ-plane and YoZ-plane, respectively. The corresponding values for Port II are 70 and 100°. The back-lobe levels for both the horizontal and vertical polarizations are about −22 dB. Compared with the antenna element without the open-ended SIC, the 3-dB beamwidths are more narrow, the back-lobe levels and cross polarization levels are improved. The simulated gain of the antenna element with the open-ended SICs are 7.3 dBi for Port I and 7.15 dBi for Port II, about 2 dBi higher the gain values of the element without the open-ended SIC.

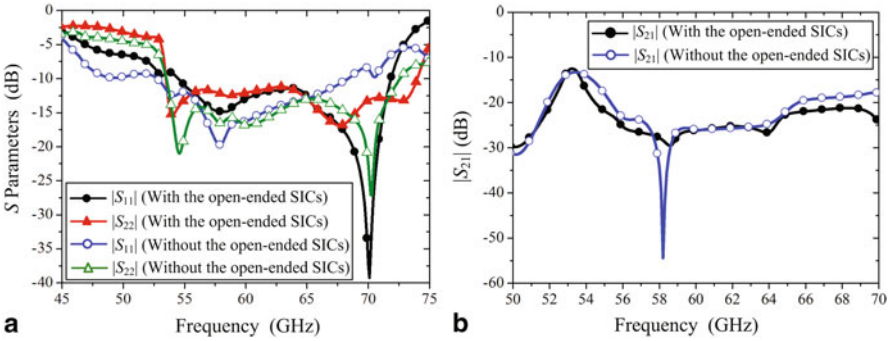

Fig. 24 Simulated S parameters of the proposed antenna element with or without the open-ended SIC. **a** $|S_{11}|$ and $|S_{22}|$, **b** $|S_{21}|$

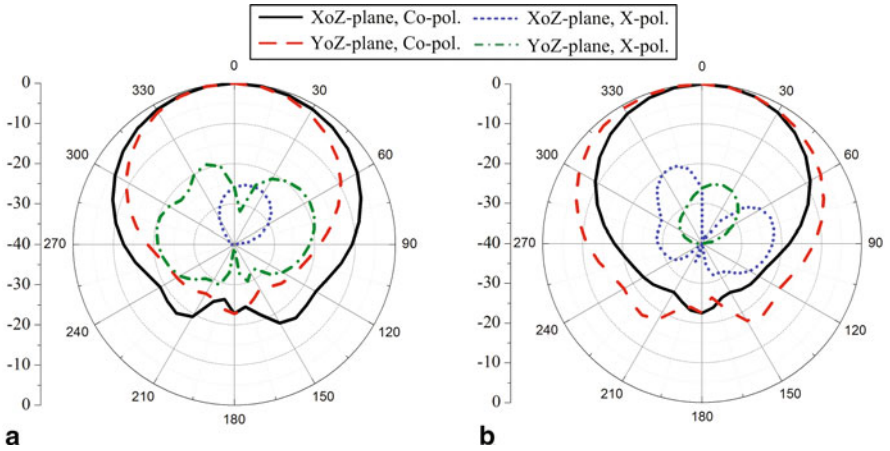

Fig. 25 Simulated radiation pattern for the proposed antenna element with the open-ended SIC at 60 GHz. **a** Port I: horizontal polarization, **b** Port II: vertical polarization

Feeding Network and GCPW-SL Transition

A compact multilayer SL feeding network consisted of two 1-to-32 power dividers is employed to achieve dual polarization characteristic of the antenna array, as Fig. 18 shows. One 1-to-32 power divider located at M2 layer is used to excite the horizontal polarization and connected to Port H. The distance between the Port H feeding network and the bottom ground (M1 layer) is 0.1 mm. The other 1-to-32 power divider located at M3 layer is used to excite the vertical polarization and connected to Port V. The distance between the Port V feeding network and the bottom ground (M1 layer) is 0.6 mm.

To make the loss from the transmission line of the feeding network, as far as possible to shorten the transmission line length is considered, a low-loss cross-over structure is used in the Port V feeding network to shorten the transmission line length

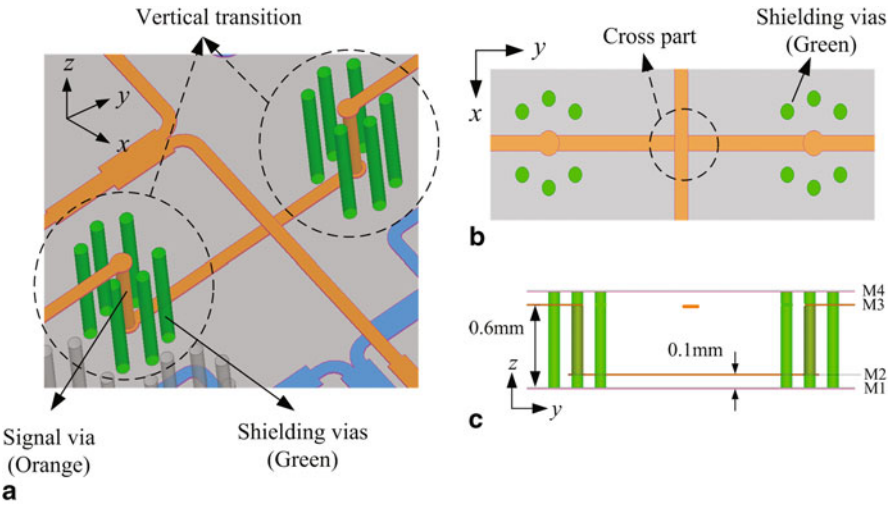

Fig. 26 Configuration of the proposed low-loss cross-over structure. **a** 3D view, **b** *Top* view, **c** *Side* view

and solve the overlap cross of the transmission line. The configuration of the low-loss cross-over structure is shown in Fig. 26. The low-loss cross-over structure consists of two vertical coaxial-like type transmission structures. The signal via connect the signal line at M2 layer and M3 layer. Surrounding the signal via, six shielding vias connected the top (M4 layer) and bottom grounds (M1 layer) are used to achieve an optimum coaxial effect and less low transmission. Figure 27 shows the simulated S parameters of the proposed cross-over structure. The simulated $|S_{11}|$ and $|S_{22}|$ are below -20 dB and $|S_{21}|$ is less than -0.4 dB from 55 to 65 GHz.

The SL fed antenna array is almost impossible to test directly. Therefore, two GCPW-SL transitions were designed as the Port H and Port V of the proposed dual-polarized antenna array, so that the antenna array can be measured with the probe station measurement as illustrated in Fig. 28. For both two different types of GCPW-SL transitions, a partial middle ground is added lower than the upper ground by 0.1 mm (1 LTCC layer) to facilitate probe pitch touching. For the Port H GCPW-SL transition, the simulated $|S_{11}|$ is below -15 dB and $|S_{21}|$ is less than -0.3 dB from 50 to 70 GHz. While, the simulated performance of the Port V GCPW-SL transition is $|S_{11}| < -18$ dB and $|S_{21}| > -0.25$ dB from 50 to 70 GHz.

The Mechanism for Performance Enhancement of Antenna Array by Loading the Open-ended SICs Structure

The electric distributions on the top surface of antenna array for Port H and Port V are simulated by HFSS software are shown in Figs. 29 and 30, so as to investigate the mechanism for performance enhancement of the antenna array loaded by the open-ended SICs structure. When the antenna is fabricated on a large size substrate

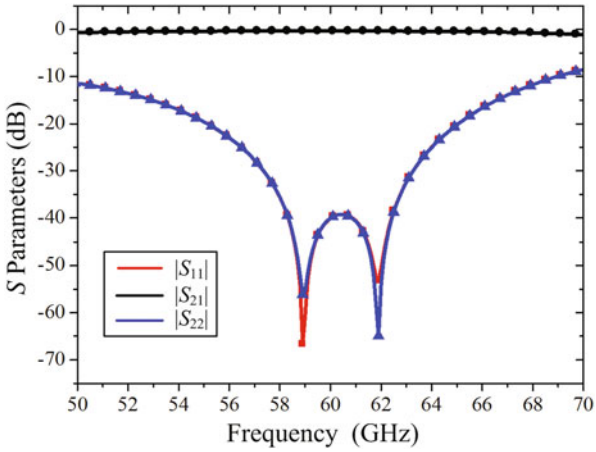

Fig. 27 Simulated *S* parameters of the proposed low-loss cross-over structure

with higher dielectric constant and thicker thickness, the strong surface waves will propagate along the substrate to weaken the radiation performance of the antenna. For Port H exciting, as Fig. 29a shows, there is strong electric field from the surface waves in the area between the antenna elements, in particular along the *y*-axis. Due to the surface wave, the original phase of each element has been changed. Therefore, the radiation performance of antenna array is deteriorated. The proposed open-ended SICs structure like an electric wall around the antenna element blocks the surface wave propagating. As Fig. 29b shows, because of the surface wave substantially suppressed, the field distribution of the radiation patch elements is improved obviously. On the other hand, the loss of the surface wave is reduced by the open-ended SICs structure, more power as the effective radiation to enhance the gain of the antenna array.

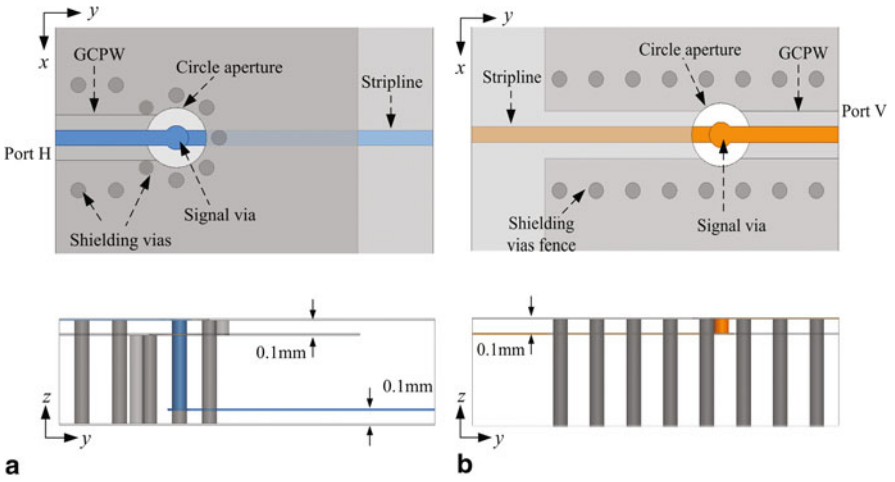

Fig. 28 Geometry of two GCPW-SL transitions. **a** Port H, **b** Port V

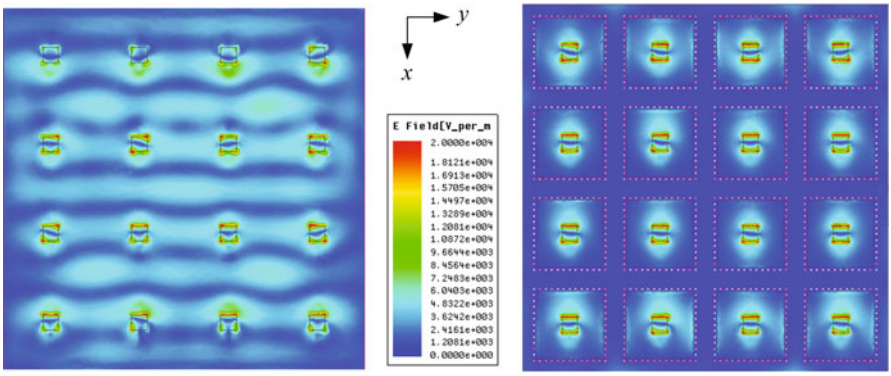

Fig. 29 Simulated electric field distributions on the *top* substrate surface of two cases arrays for Port H. **a** Without the open-ended SICs structure, **b** With the open-ended SICs structure

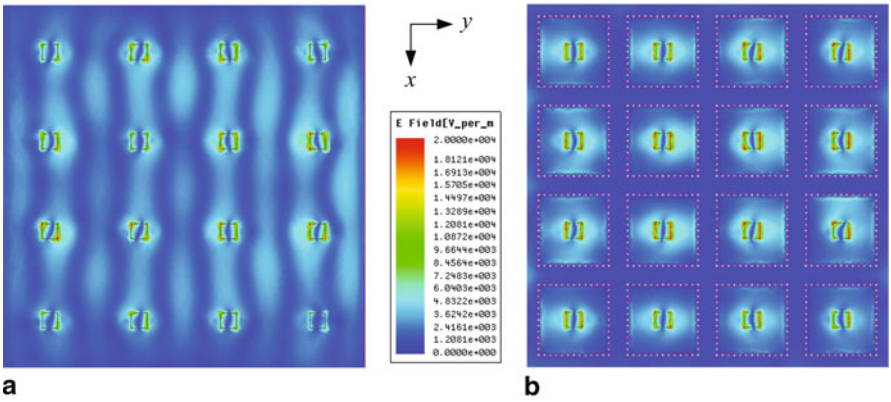

Fig. 30 Simulated electric field distributions on the *top* substrate surface of two cases arrays for Port V. **a** Without the open-ended SICs structure, **b** With the open-ended SICs structure

Similarly, for Port V exciting, strong electric field from the surface waves existing in the area between the antenna elements in Fig. 30a, in particular along the x-axis, disturb the original phase of each element. For this reason, the radiation performances of antenna array are deteriorated. After employing the open-ended SICs structure, as Fig. 30b shows, the surface wave is substantially suppressed to result in the gain enhancement of the antenna array.

Simulated and Measured Results

Figure 31 shows the photograph of the fabricated antenna array with the open-ended SICs and two GCPW-SL transitions.

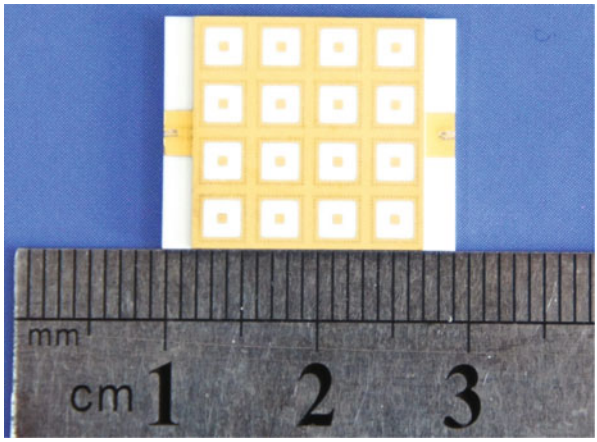

Fig. 31 Photograph of the proposed fabricated dual-polarized antenna array with open-end SICs

The measured and simulated S parameters of the proposed antenna array are illustrated in Fig. 32. The simulated 10-dB impedance bandwidths are $\sim 19.1\,\%$ with respect to 60.25 GHz from 54.5 to 66 GHz for Port H, and $\sim 24.4\,\%$ with respect to 61.5 GHz from 54 to 69 GHz for Port V, respectively. The measured reflection coefficients of antenna array is slightly worse than the simulated values. The discrepancy could come from the LTCC fabrication tolerance and substrate shrink, the inaccuracy of the dielectric permittivity, and even from the touching position of the Ground-Signal-Ground (GSG) probe influence.

Figure 33 shows the measured and simulated input ports isolation of the proposed dual-polarized antenna array. It can be seen that, the simulated $|S_{21}|$ of the antenna array is less than -25 dB from 58.5 to 65 GHz. Whereas, the measured isolation $|S_{21}|$ is below -20 dB over the frequency range from 58.5 to 65 GHz.

The measured gain of the proposed antenna array for Port H and Port V are plotted in Fig. 34, and compared with the simulated results. Considering the metal chuck and the different calibrations needed for this setup (standard horn antenna, waveguide

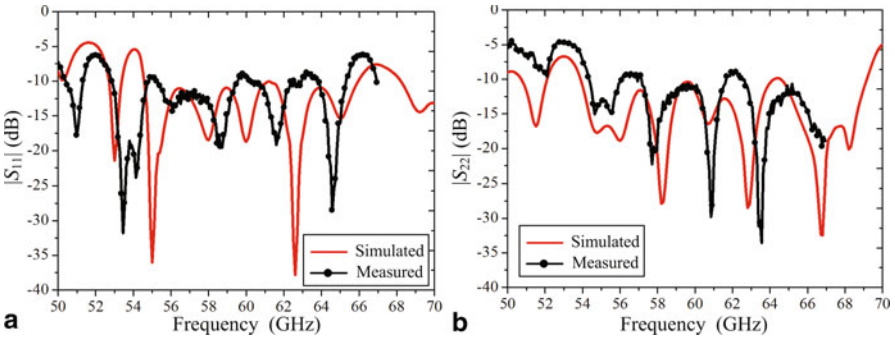

Fig. 32 Measured and simulated S parameters of the antenna array, **a** Port H ($|S_{11}|$), **b** Port V ($|S_{22}|$)

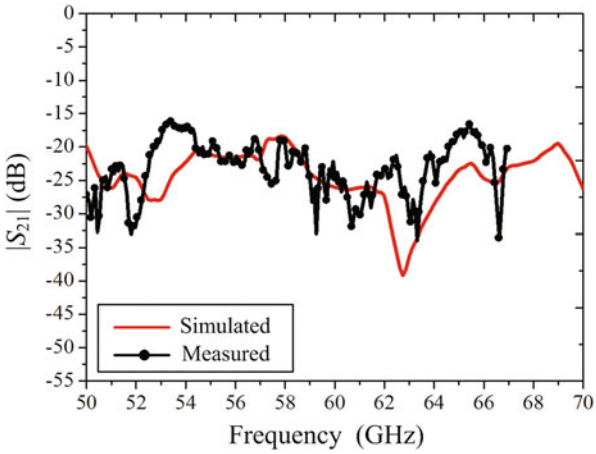

Fig. 33 Measured and simulated ports isolation ($|S_{21}|$) of the antenna array

to coaxial adapter, GSG probes, and misalignment), the accuracy of the measured gain is estimated to be 1 dB in the frequency band. The simulated and measured gain results are 18.5 and 17.1 dBi for Port H, respectively. The measured 3-dB gain bandwidth of the proposed array for Port H is from 56 to 67 GHz. As Fig. 22b shows, the simulated and measured gain results are 17.8 and 16.6 dBi for Port V, respectively. The measured 3-dB gain bandwidth of the proposed array for Port V is from 55 to 66 GHz. compared with the simulated results, the gain is dropped about 1.4 dB. It is mainly caused by three following reasons: (1) the deterioration of impedance matching; (2) the deviation of the LTCC substrate dielectric and the conductivity of the metallization material; (3) The shrinking of LTCC fabrication.

The measured and simulated co-pol and cross-pol radiation patterns of the proposed dual-polarized antenna array in two principal planes (XoZ-plane and YoZ-plane) at 60 GHz for Port H and Port V are shown in Fig. 35, respectively. For Port H horizontal polarization, as Fig. 35a shows, the simulated and measured

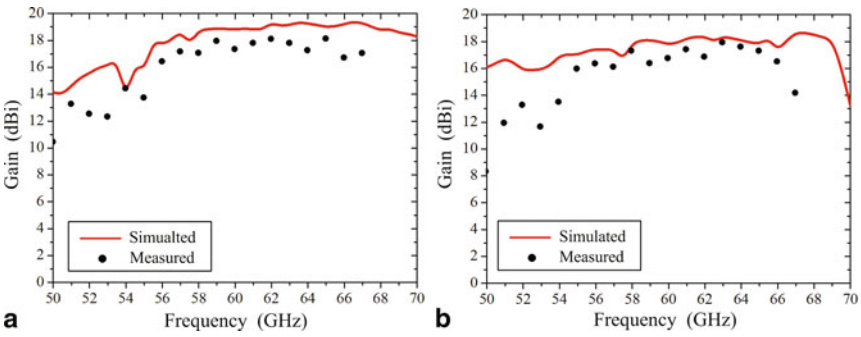

Fig. 34 Measured and simulated gain of the antenna array, **a** Port H: *horizontal* polarization, **b** Port V: *vertical* polarization

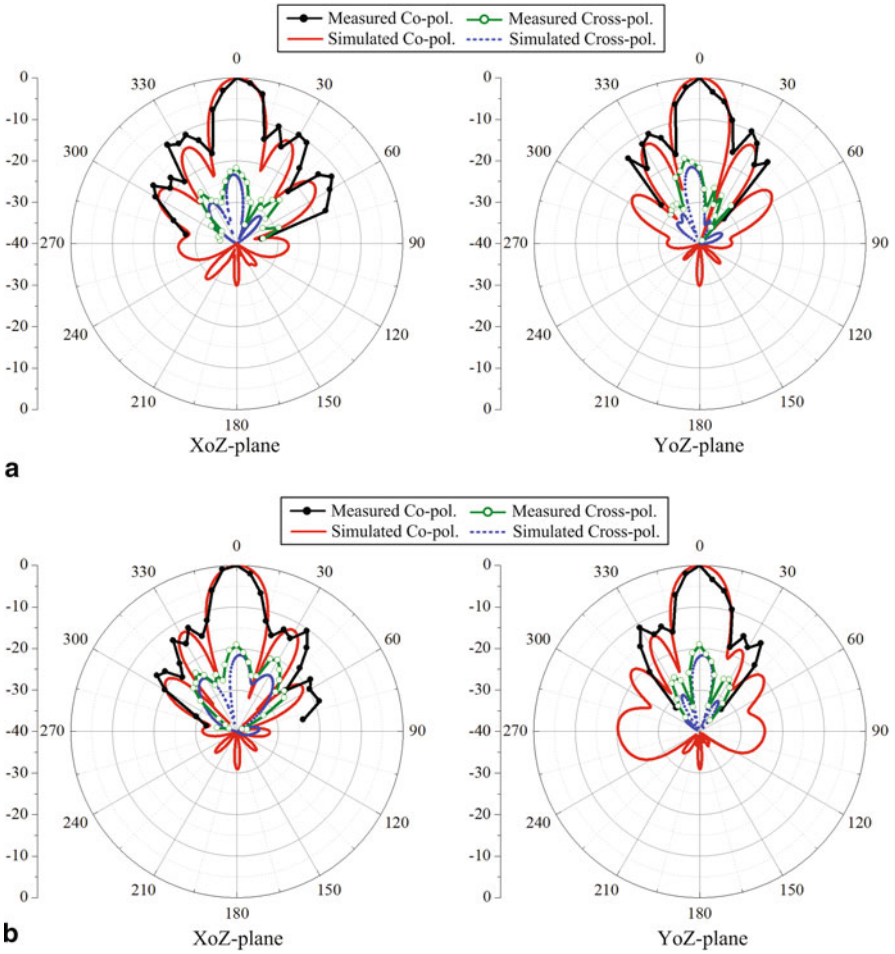

Fig. 35 Measured and simulated radiation patterns of the proposed antenna array at 60 GHz, **a** Port H for *horizontal* polarization, **b** Port V for *vertical* polarization

cross-polarization levels are almost −22.3 and −19.1 dB in two principal planes. For Port V vertical polarization, as Fig. 35b shows, the simulated and measured cross-polarization levels are about −21.6 and −19.5 dB in two principal planes, respectively.

A 4 × 4 LTCC dual-polarized L-probe patch antenna array with the open-ended SICs structure for 60 GHz wireless communication applications has been designed and tested. The proposed 60-GHz dual-polarized antenna array has compact size, wide bandwidth, good isolation, high gain and wide 3-dB gain bandwidth by employed the multilayer SL feeding network, "differential feed" L-probe approach, and open-ended SICs.

References

1. P. Smulders, Exploring the 60 GHz band for local wireless multimedia access: prospects and future directions. IEEE. Commun. Mag. **40**(1), 40–147 (Jan. 2002)
2. A. Sadri, 802.15.3c usage model document. IEEE 802.15-06-0055-14-003c (May 2006)
3. Y.P. Zhang, D. Liu, Antenna-on-chip and antenna-in-package solutions to highly integrated millimeter-wave devices for wireless communications. IEEE. Trans. Antennas Propag. **57**(10), 2830–2841 (Oct. 2009)
4. T.S. Rappaport, J.N. Murdck, F. Gutierrez, State of the art in 60-GHz integrated circuits and systems for wireless communications. Proc. IEEE. **99**(8), 1390–1436 (Aug. 2011)
5. D. Liu, Y.P. Zhang, Integration of antenna arrays in chip package for 60-GHz radios. Proc. IEEE. **100**(7), 2364–2371 (Jul. 2012)
6. R.R. Tummala, M. Swaminathan, M.M. Tentzeris, J. Laskar, G.-K. Chang, S. Sitaraman, D. Keezer, D. Guidotti, Z.R. Huang, K. Lim, L.X. Wan, S.K. Bhattacharya, V. Sundaram, F.H. Liu, P.M. Raj, The SOP for miniaturized, mixed-signal computing, communication, and consumer systems of the next decade. IEEE Trans. Adv. Packag. **27**(2), 250–267 (May 2004)
7. Y.P. Zhang, M. Sun, D. Liu, Y. Lu, Dual grid antenna arrays in a thin-profile package for flip-chip interconnection to highly integrated 60-GHz radios. IEEE Trans. Antennas Propag. **59**(4), 1191–1199 (Apr. 2011)
8. H. Chu, Y.-X. Guo, Z. Wang, 60-GHz LTCC wideband vertical Off-Center dipole antenna and arrays. IEEE. Trans. Antennas Propag. **61**(1), 153–161 (Jan. 2013)
9. J. Xu, Z.N. Chen, X. Qing, W. Hong, Bandwidth enhancement for a 60 GHz substrate integrated waveguide fed cavity antenna array on LTCC. IEEE. Trans. Antennas Propag. **59**(3), 826–832 (Mar. 2012)
10. L. Wang, Y.-X. Guo, W.X. Sheng, Wideband high-gain 60-GHz LTCC L-probe patch antenna array with a soft surface. IEEE. Trans. Antennas Propag. **61**(4) 1802–1809 (Apr. 2013)
11. H. Sun, Y.-X. Guo, Z. Wang, 60-GHz circularly polarized U-slot patch antenna array on LTCC. IEEE. Trans. Antennas Propag. **61**(1), 430–435, (Jan. 2013)
12. M. Sun, Y.Q. Zhang, Y.-X. Guo, M.F. Karim, L.C. Ong, M.S. Leong, Integration of circular polarized array and LNA in LTCC as a 60-GHz active receiving antenna. IEEE. Trans. Antennas Propag. **59**(8), 3083–3089 (Aug. 2011)
13. C. Liu, Y.-X. Guo, X. Bao, S.Q. Xiao, 60-GHz LTCC integrated circularly polarized helical antenna array. IEEE. Trans. Antennas Propag. **60**(3), 1329–1335 (Mar. 2012)
14. A.E.I. Lamminen, J. Säily, A.R. Vimpari, 60-GHz patch antennas and arrays on LTCC with embedded-cavity substrates. IEEE. Trans. Antennas Propag. **56**(9), 2865–2874 (Sep. 2008)
15. I. K. Kim, N. Kidera, S. Pinel, J. Papapolymerou, J. Laskar, J.-G. Yook, M.M. Tentzeris, Linear tapered cavity-backed slot antenna for millimeter-wave LTCC modules. IEEE. Antennas Wireless. Propag. Lett. **5**, 175–178 (2006)
16. S.B. Yeap, Z.N. Chen, X. Qing, Gain-enhanced 60-GHz LTCC antenna array with open air cavities. IEEE. Trans. Antennas Propag. **59**(9), 3470–3473 (Sep. 2011)
17. A.E.I. Lamminen, A.R. Vimpari. J. Säily, UC-EBG on LTCC for 60-GHz frequency band antenna applications. IEEE. Trans. Antennas Propag. **57**(10), 2904–2912 (Oct. 2009)
18. Y. Li, Z.N. Chen, X. Qing, Z. Zhang, J. Xu, Z. Feng, Axial ratio bandwidth enhancement of 60-GHz substrate integrated waveguide-fed circularly polarized LTCC antenna array. IEEE. Trans. Antennas Propag. **60**(10), 4619–4626 (Oct. 2012)
19. K.M. Luk, C.L. Mak, Y.L. Chow, K.F. Lee, Broadband microstrip patch antenna. Electron. Lett. **34**, 1442–1443 (July 1998)
20. C.L. Mak, K.M. Luk, K.F. Lee, Y.L. Chow, Experimental study of a microstrip antenna with an L-shaped probe. IEEE. Trans. Antennas Propag. **48**, 777–783 (May 2000)
21. Y.-X. Guo, C.L. Mak, K.M. Luk, K.F. Lee, Analysis and design of L-probe proximity fed patch antenna. IEEE. Trans. Antennas Propag. **49**(2), 145–149 (Feb. 2001)
22. P.-S. Kildal, Artificially soft and hard surfaces in electromagnetic. IEEE. Trans. Antennas Propag. **38**(10), 1537–1544 (Oct. 1990)

23. Z. Ying, P.-S. Kildal, Study of different realizations and calculation models for soft-surfaces by using vertical monopole on soft disk as test bed. IEEE. Trans. Antennas Propag. **44**(11), 1474–1481 (Nov. 1996)
24. R. Li, G. DeJean, M.M. Tentzeris, J. Papapolymerou, J. Laskar, Radiation-pattern improvement of patch antenna on a large-size substrate using a compact soft-surface structure and Its realization on LTCC multilayer technology. IEEE. Trans. Antennas Propag. **53**(1), 200–208 (Jan. 2005)
25. Y.-X. Guo, K.M. Luk, K.F. Lee, Broadband dual polarization patch element for cellular-phone base stations. IEEE. Trans. Antennas Propag. **50**(2), 251–253 (Feb 2002)
26. L. Bian, Y.-X. Guo, L.C. Ong, X.Q. Shi, Wideband circularly-polarized patch antenna. IEEE. Trans. Antennas Propag. **54**(9), 2682–2686 (Sep. 2006)
27. H. Wong, K.-L. Lau, K.-M. Luk, Design of dual-polarized L-probe patch antenna arrays with high isolation. IEEE. Trans. Antennas Propag. **52**(1), 45–52 (Jan. 2004)
28. Y.-X, Guo, K.-W. Khoo, L.C. Ong, Wideband dual-polarized patch antenna with broadband baluns. IEEE. Trans. Antennas Propag. **55**(1), 78–83 (Jan. 2004)
29. K.L. Lau, K.M. Luk, A. wideband dual-polarized L-Probe stacked patch antenna array. IEEE. Lett. **6**, 529–532 (2007)
30. J. Heyen, A. Gordiyenko, P. Heide, A.F. Jacob, Vertical feedthroughs for millimeter-wave LTCC modules. In IEEE Eur. Microw. Conf., Munich, Germany, pp. 411–414 (Oct. 2003)
31. C.-C. Tsai, T.-S. Chen, T.-Y. Huang, Y.A. Hsu, R.-B. Wu, Design of microstrip-to-microstrip via transition in multilayered LTCC for frequencies up to 67 GHz. IEEE Trans. Compon. Packag. Manufactur. Tech. **1**(4), 595–600 (April. 2011)